J. Electrochem. Sci. Eng. **16** (2026) 3447; https://doi.org/10.5599/jese.3447

Open Access : : ISSN 1847-9286
https://pub.iapchem.org/ojs/index.php/JESE

Original scientific paper

Co-detection of isoproterenol and uric acid in biological and pharmaceutical samples at modified carbon paste electrode

Marib Ismail Ali[1,✉], Ghofran Ali[2] and Noor Hameed Neama Aziz[3]

[1]*Ministry of Education, General Directorate of Education, Salah Al-Din, Iraq*
[2]*Ministry of Education, General Directorate of Education, Najaf, Iraq*
[3]*Ministry of Education, Directorate of Education Thi-Qar, 64001, Iraq*

Corresponding Author: ✉ *suhaebh1@gmail.com*

Received: May 18, 2026; Accepted: June 3, 2026; Published: August 11, 2026

Abstract

In this study, cyclic voltammetry was used to examine electrochemical characteristics of a carbon paste electrode (CPE) modified with a manufactured Ni-based 1,3,5-benzenetricarboxylate metal-organic framework nanostructure/graphene oxide nanocomposite (NBM/Go/CPE). The modified electrode demonstrated outstanding electrocatalytic activity toward isoproterenol (IPT). The oxidation potential of IPT would drop to approximately 170 mV at the NBM/Go/CPE, compared with that at an unmodified CPE. Two linear dynamic ranges, 0.05 to 480.0 µM IPT, were demonstrated using differential pulse voltammetry. The IPT detection limit was 0.015 µM. To determine IPT in the presence of uric acid (UA), the selectivity of the developed electrochemical sensor was also examined. Ultimately, NBM/Go/CPE was used to detect IPT and UA in drug samples and human urine, yielding satisfactory findings.

Keywords

Heart attacks; bronchitis; cardiac shock; voltammetry; catecholamines; drug analysis; urine analysis

Introduction

The medication isoproterenol (IPT) serves as a treatment for heart attacks, bronchitis, cardiac shock, allergic reactions and primary pulmonary hypertension. The medication's excessive dosage leads to two dangerous outcomes, which include arrhythmias and cardiac failure [1,2]. IPT causes cardiovascular side effects because of its negative effects on the body. Patients who experience tachycardia from IPT face an increased risk of developing cardiac dysrhythmias [1,2]. Chemically modified electrodes have been used as effective analytical tools to measure IPT due to their direct sensitivity to it [3]. The electrochemical method offers various advantages through modified electrodes, which include enduring stability, high sensitivity, lower overpotential and consistent performance in electroanalysis [4,5].

One of the key macromolecules found in bodily fluids is UA, the final metabolic product of purine metabolism in the liver [6]. A number of clinical disorders, including renal injury, gout, and Lesch-Nyhan illnesses, can cause abnormal UA levels [7]. Additionally, a condition known as hyperuricemia results if UA is not eliminated from the body or if UA production increases [8]. Chemiluminescence [9] and electrochemical techniques [10] are two techniques reported for UA analysis. However, UA significantly interferes with the determination of IPT. Therefore, to determine IPT, especially when UA is present, an appropriate detection approach that is selective, straightforward, affordable, quick, sensitive, and accurate is needed [10].

A study on a liquid carbon electrode intended to replace mercury in polarography led to the development of CPEs in the 1950s as a straightforward yet effective electrode material [11]. CPEs have been the subject of extensive research in biological, pharmacological and environmental analysis for the past 70 years [12,13].

In short, the CPE composite consists of a binder (mineral oil) and a conductive material, usually graphite, because of its high conductivity and low cost [14].

Emerging porous crystalline materials (PCMs) include metal-organic frameworks (MOFs) [15]. These frameworks offer the freedom to customize pore size and particular applications. MOFs create networks of linked pores and channels by assembling these components. Due to their favourable characteristics, MOFs have shown great promise as functional materials in a variety of sectors. These frameworks exhibit appealing compositions, surfaces, topologies, and more [15]. MOFs can be used in a variety of applications, and sensing is a significant application of MOFs, and these frameworks have proven capable of recognizing target molecules in a variety of samples [16,17].

The low electrical conductivity, which characterizes most metal-organic frameworks, poses obstacles that prevent their use in electrochemical sensor applications. Researchers continue their work to demonstrate that MOF electrical conductivity can be improved by combining MOFs with various nanostructures, thereby enhancing their performance in electrochemical sensors [18]. The electrical conductivity of MOF-based composites demonstrates their ability to combine the advantages of metal-organic frameworks and conductive materials. Among the various nanomaterials suggested for electrochemical sensor applications, graphene oxide (GO) has become an essential carbon nanostructured material that brings both effectiveness and value [19]. The oxidized derivative of graphene, known as graphene oxide, exhibits exceptional properties [19]. The oxygen functional groups on GO's surface provide multiple sites for MOF binding, creating a nanocomposite material that functions as an efficient electrode system [20]. Combining MOFs with GO to form a composite material provides high sensitivity for analysing specific analytes via electrochemical methods [21].

In this work, an appropriate and effective NBM/Go/CPE is fabricated for IPT determination. NBM/Go/ /CPE can determine IPT, thanks to its outstanding electrocatalytic performance. Additionally, the NBM/ /Go/CPE shows a good response for the simultaneous detection of IPT and UA. Additionally, the new sensor proved more effective in identifying these substances in pharmaceutical and biological samples.

Experimental

Apparatus and chemicals

A PGSTAT Autolab 302N potentiostat-galvanostat was utilized for all voltammetric and chronoamperometric measurements. The working electrodes (WEs), counter electrode (CE), and reference electrode (RE) of this potentiostat-galvanostat are unmodified CPE or NBM/Go/CPE, platinum wire, and Ag/AgCl (inner solution: 3.0 M KCl), respectively. Sigma-Aldrich and Merck supplied all of the compounds.

Synthesis of nanocomposite

The following solvothermal process was used to create the nanocomposite. In short, 60 mL of DMF was mixed with 0.5 mmol of benzene-1,3,5-tricarboxylic acid and 3.0 mmol of $Ni(NO_3)_2 \cdot 6H_2O$ while being magnetically stirred for 15 minutes at room temperature. After that, 0.015 g of GO was added to the solution mentioned above, and the mixture was stirred for half an hour. To obtain a homogeneous suspension, ultrasonication was performed for 60 minutes after stirring. The resulting suspension was then placed in an autoclave and heated to 160 °C for 15 hours to undergo solvothermal treatment. The prepared precipitates were separated by centrifugation, washed with ethanol and DMF, and finally dried.

Preparation of NBM/Go/CPE

Graphite powder and nanocomposite were weighed in the appropriate amounts and thoroughly mixed in a mortar to prepare 1.0 g of CP. The required amount of paraffin oil was then added to the above mixture, and the components were further ground to obtain a uniform carbon paste. The resulting NBM/Go/CPE was then poured into the end of a Teflon tube, which served as the electrode body. NBM/Go/CPE was created by inserting a copper wire into the middle of the Teflon tube. It should be noted that, to achieve a clean surface prior to measurements, the surface electrode was periodically polished on paper. Additionally, the unmodified CPE was prepared in a manner similar to that of the NBM/Go/CPE to enable comparative experiments.

Procedure of real samples preparation

After diluting 1 mL of an IPT ampoule to 20 mL using buffer, varying volumes of the diluted solution were poured into a series of 50 mL volumetric flasks. The suggested strategy examines the IPT content.

The urine sample (20 mL) was centrifuged at 2000 rpm for 15 minutes. A 50 mL volumetric flask was then filled with varying volumes of the solution. Different concentrations of IPT and UA were added to the diluted urine sample.

Electrochemical methodology

CV was performed in the potential range of -50 to 800 mV at a scan rate (v) of 50 mV s^{-1}. The oxidation mechanism of IPT was examined at the surface of an unmodified CPE and NBM/Go/CPE. DPV measurements to determine IPT were recorded on the NBM/Go/CPE surface from 140 to 610 mV.

Results and discussion

Electrochemical behaviour of isoproterenol at unmodified carbon paste electrode and Ni-based 1,3,5--benzenetricarboxylate metal-organic framework nanostructure/graphene oxide nanocomposite

In the buffer solution containing IPT, the electrocatalytic performance of NBM/Go/CPE was compared with that of unmodified CPE (Figure 1). A poor oxidation peak (I_{pa} = 4.0 µA) was found at an oxidation peak potential (E_{pa}) of 540 mV for IPT on the unaltered CPE. The oxidation of IPT was detected at a lower E_{pa} (370 mV) with I_{pa} = 11.0 µA at the surface of NBM/Go/CPE in comparison to unmodified CPE, which was attributed to the favourable characteristics of BTC MOF NSs and GOs.

http://doi.org/10.5599/jese.3447

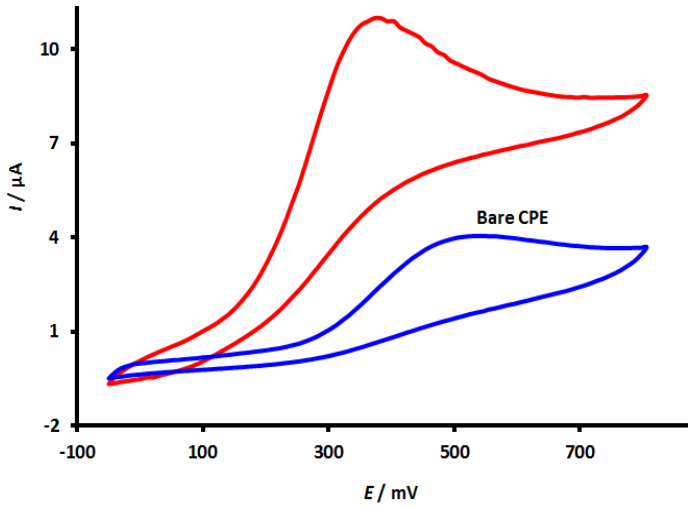

Figure 1. *CV responses of bare CPE and NBM/Go/CPE in the buffer solution containing 100.0 µM IPT at* v *= 50 mV* s^{-1}

Effect of scan rate

The purpose of this part was to examine how *v* affected the electrochemical oxidation process of IPT at NBM/Go/CPE. The cyclic voltammetry responses of NBM/Go/CPE in detecting 100.0 µM IPT were recorded at different scan rates (Figure 2A). It is evident from the results shown in Figure 2 that the I_{pa} increases as *v* increases from 10 to 500 mV s^{-1}. Additionally, as shown in Figure 2B, there is a linear correlation between the peak currents of cyclic voltammograms and the square root of the *v*. Significantly, this study showed that diffusion controls the oxidation process of IPT.

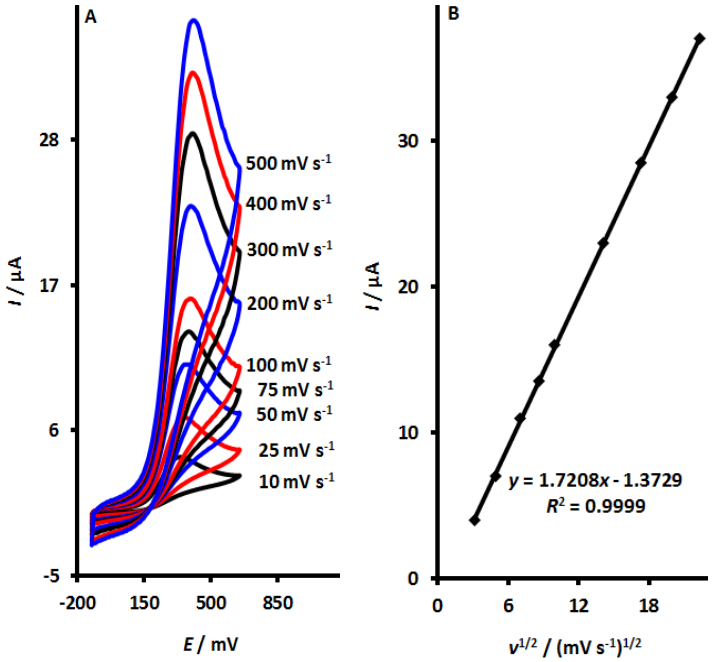

Figure 2*. (A) CV responses of NBM/Go/CPE in the solution containing 100.0 µM IPT at various scan rates. (B) Plot of the corresponding peak currents against* $v^{1/2}$ *for each of the recorded CVs*

Chronoamperometric studies

The chronoamperograms obtained at NBM/Go/CPE in response to different IPT concentrations in the buffer solution by applying a single potential step (865 mV) for 25 s are shown in Figure 3A. The purpose of this investigation was to ascertain the diffusion coefficient (*D*) value related to the IPT oxidation process at the modified CPE. The recorded chronoamperograms show how current

depends on time. The relationship between current and $t^{-1/2}$ showed straight lines over a brief period for each recorded chronoamperogram at a given IPT concentration (Figure 3B). The matching slopes from Cottrell plots (Inset A) were then plotted against IPT concentrations (Figure 3C). The *D* value for IPT oxidation at NBM/Go/CPE was predicted to be 1.88×10^{-6} cm^2 s^{-1}.

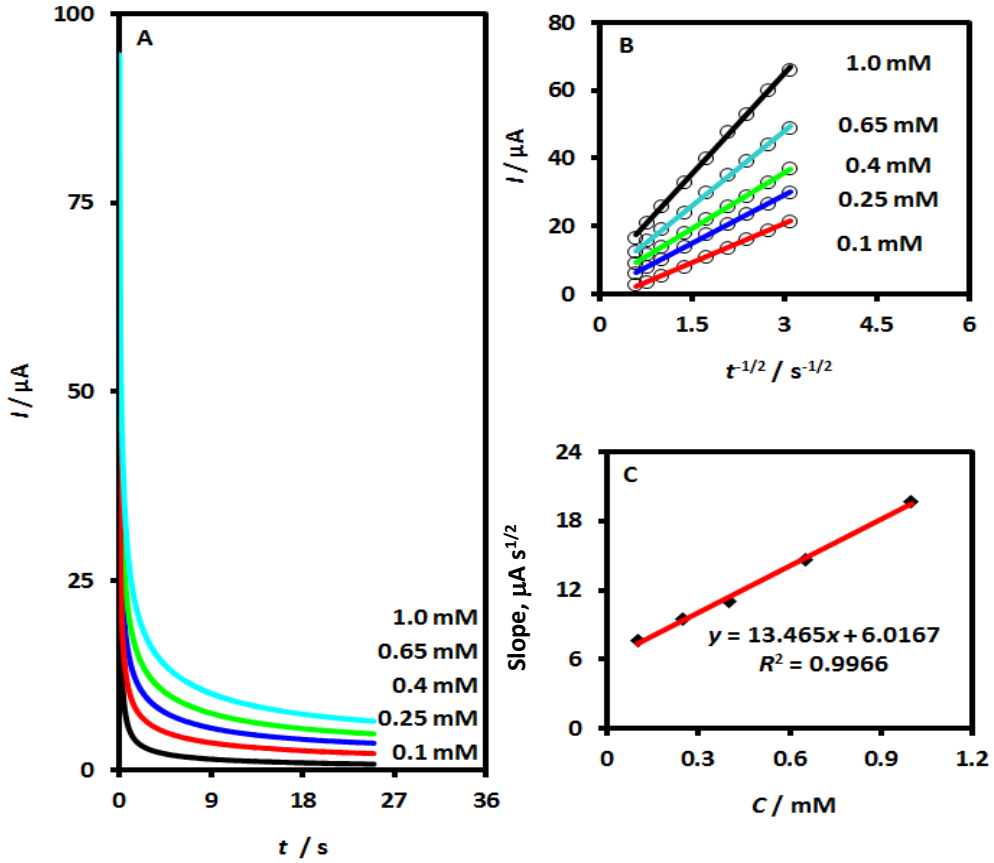

Figure 3: *(A) The chronoamperometric responses of NBM/Go/CPE in the solution containing different concentrations of IPT (B) plot of the corresponding slopes obtained from* I vs. $t^{-1/2}$ *plots against the concentrations of IPT and (C) plot of* I vs. $t^{-1/2}$ *in the specific time range of each recorded chronoamperogram*

DPV measurements for quantitative analysis of isoproterenol

The differential pulse voltammetry (DPV) responses of NBM/Go/CPE during the electrochemical oxidation process at different IPT concentrations were quantitatively measured (Figure 4A).

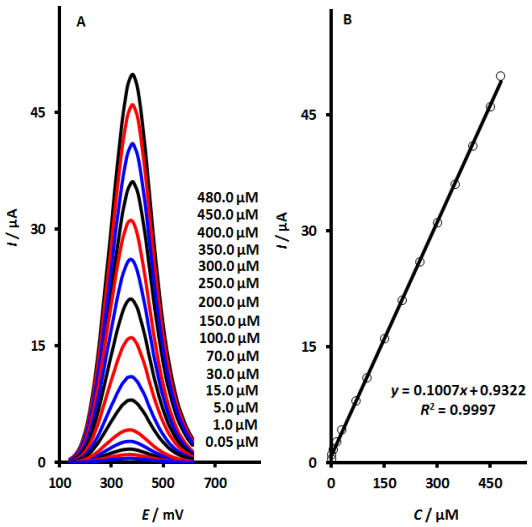

Figure 4. *(A) DPV responses of NBM/Go/CPE for various concentrations of IPT. (B) Calibration plot of IPT (plot of peak currents against concentrations of IPT)*

According to the DPVs shown in Figure 4A, an increase in IPT concentration increases IPT's I_{pa}. Additionally, as shown in Figure 4B, the anodic peak currents of the respective voltammograms were proportional to the IPT concentrations. A broad linear range for IPT measurement, from 0.05 to 480.0 µM, was displayed in the calibration plot. At the NBM/Go/CPE, the sensitivity and LOD values for IPT determination were 0.1007 µA μM^{-1} and 0.015 µM, respectively.

Differential pulse voltammetry measurements of isoproterenol in the presence of uric acid

Additionally, the simultaneous measurement of IPT and UA on the NBM/Go/CPE was investigated in another study. To conduct this experiment, their concentration was varied concurrently, and the corresponding DPVs were recorded (Figure 5A). Two distinct oxidation peaks for IPT and UA were observed at 370 and 530 mV, respectively, as shown in the DPVs in Figure 5A. The corresponding peak currents associated with the oxidation of IPT and UA likewise increased linearly as their concentrations were raised concurrently. When the concentration of UA was increased from 1.0 to 600.0 µM, the anodic peak currents of UA increased linearly (Figure 5C). Additionally, when the concentration of IPT was increased from 1.0 to 480.0 µM, the anodic peak currents of IPT increased linearly (Figure 5B).

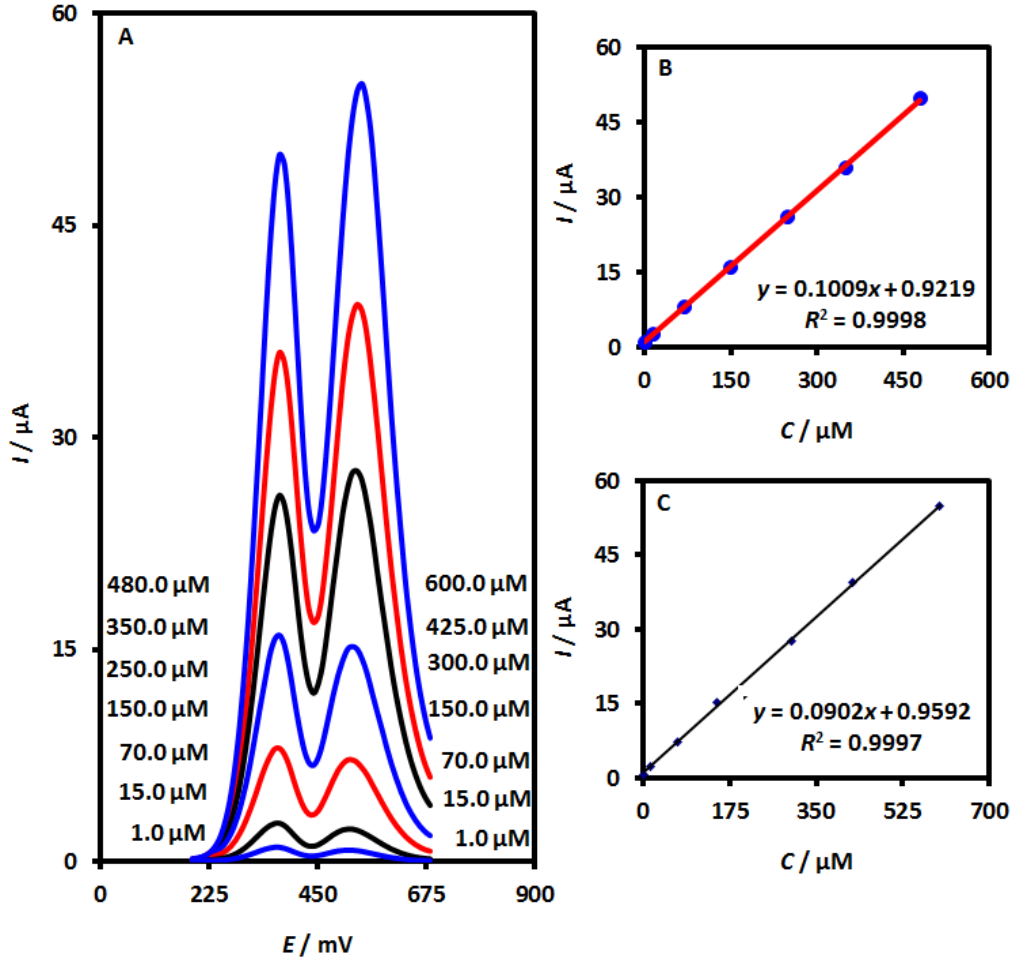

Figure 5. *(A) DPV responses of NBM/Go/CPE for various concentrations of IPT and UA. Calibration plots of IPT (B) and UA (C)*

Practical application of the Ni-based 1,3,5-benzenetricarboxylate metal-organic framework nanostructure/graphene oxide nanocomposite sensor

Urine and IPT injection samples were examined in order to assess the practical use of the voltammetric (DPV) method using the NBM/Go/CPE sensor for IPT and UA determination in actual samples.

First, IPT injection and urine samples without a spiked standard solution of IPT and UA were examined, and the concentration of IPT and UA in these samples was determined. The tests then continued to spike these samples with standard solutions of IPT and UA at specific concentrations, and the accompanying DPVs were noted. The concentrations of IPT and UA detected in these samples, along with the recovery percentages and relative standard deviation (RSD), are shown in Table 1. Table 1 shows that the examined samples' IPT and UA recoveries ranged from 97.1 to 104.3 %, which is satisfactory. It shows how accurate the created process is. Furthermore, the RSD were ≤3.5 %, indicating that these measurements were highly precise. It should be mentioned that this proposed method was highly effective in determining IPT and UA in biological and pharmaceutical materials.

Table 1. *Detection of IPT and UA in various spiked samples (IPT injection and urine) using NBM/Go/CPE for real sample analysis*

Sample	Concentration, μM				Recovery, %		RSD, %	
	Spiked		Found					
	IPT	UA	IPT	UA	IPT	UA	IPT	UA
IPT injection	0	0	3.9	-	-	-	3.4	-
	2.0	5.5	5.8	5.7	98.3	103.6	2.2	3.5
	3.0	7.5	7.2	7.4	104.3	98.7	1.9	2.7
Urine	0	0	-	4.7	-	-	-	
	5.0	2.0	5.1	6.6	102.0	98.5	3.3	2.9
	7.0	3.0	6.8	8.0	97.1	103.9	2.1	2.6

Conclusion

NBM/Go/CPE was used to electrochemically determine IPT. The Ni-BTC MOF NSs/GO/CPE had a superior CV response to IPT in comparison to other electrodes. It dramatically raised IPT's oxidation current and decreased its oxidation potential. Additionally, a linear response spanning the concentration range of 0.05 to 480.0 μM, with an LOD of 0.015 μM, was obtained from quantitative DPV measurements. Lastly, IPT and UA were determined in urine and IPT injection samples using the NBM/Go/CPE. Acceptable recoveries ranged from 97.1 to 104.3 %, and RSDs were no greater than 3.5 %, indicating the sensor's suitability for IPT and UA measurements in actual samples.

Funding: *Not applicable.*

References

[1] M. Zhao, M. Han, L. Liang, Q. Song, X. Li, Y. Du, D. Hu, Y. Cheng, Q.K. Wang, T. Ke, Mog1 deficiency promotes cardiac contractile dysfunction and isoproterenol-induced arrhythmias associated with cardiac fibrosis and Cx43 remodeling, *Biochimica et Biophysica Acta (BBA)-Molecular Basis of Disease* **1868** (2022) 166429. https://doi.org/10.1016/j.bbadis.2022.166429

[2] W. Liu, E. Qaed, W. Aldahmash, M. A. Mahyoub, W. A. Hailan, A. K. Alwesabi, Z. Tang, Phosphocreatine attenuates isoproterenol-induced cardiac fibrosis via activation of the Nrf2/ARE antioxidant pathway and preservation of endothelial integrity, *Archives of Biochemistry and Biophysics* **779** (2026) 110776. https://doi.org/10.1016/j.abb.2026.110776

[3] P. Solich, C. K. Polydorou, M. A. Koupparis, C. E. Efstathiou, Automated flow-injection spectrophotometric determination of catecholamines (epinephrine and isoproterenol) in pharmaceutical formulations based on ferrous complex formation, *Journal of Pharmaceutical and Biomedical Analysis* **22** (2000) 781-789. https://doi.org/10.1016/S0731-7085(00)00291-0

[4] M. Keyvanfard, K. Alizad, Determination of isoproterenol in pharmaceutical and biological samples using a pyrogallol red multiwalled carbon nanotube paste electrode as a sensor, *Chinese Journal of Catalysis* **37** (2016) 579-583. https://doi.org/10.1016/S1872-2067(15)61036-1
[5] M. Mazloum-Ardakani, N. Rajabzadeh, A. Dehghani-Firouzabadi, A. Benvidi, B. B. Mirjalili, L. Zamani, Development of an electrode modified on the basis of carbon nanoparticles and reduced graphene oxide for simultaneous determination of isoproterenol, uric acid and tryptophan in real samples, *Journal of Electroanalytical Chemistry* **760** (2016) 151-157. https://doi.org/10.1016/j.jelechem.2015.11.033
[6] R. Bao, Q. Chen, Z. Li, D. Wang, Y. Wu, M. Liu, Y. Zhang, T. Wang, Eurycomanol alleviates hyperuricemia by promoting uric acid excretion and reducing purine synthesis, *Phytomedicine* **96** (2022) 153850. https://doi.org/10.1016/j.phymed.2021.153850
[7] K. K. Ray, S. J. Nicholls, A. M. Lincoff, N. Li, H. A. Powell, P. M. Herout, L. Bloedon, S. E. Nissen, Association of uric acid-lowering therapies on gout frequency with bempedoic acid: clinical insights from CLEAR outcomes, *JACC: Advances* **4** (2025) 102207. https://doi.org/10.1016/j.jacadv.2025.102207
[8] W. Wang, Z. Min, C. Luo, M. Yang, L. Chen, Extract of Clematis hexapetala regulates uric acid metabolism, alleviates renal inflammation and fibrosis via the PI3K/AKT/NF-κB signaling pathway, and improves hyperuricemia in mice, *Journal of Ethnopharmacology* **367** (2026) 121698. https://doi.org/10.1016/j.jep.2026.121698
[9] S. Karimi, M. Amjadi, Investigation of the chemiluminescence behavior of Ti_3C_2 MXene quantum dots as a sensing platform for uric acid, *Microchemical Journal* **207** (2024) 112068. https://doi.org/10.1016/j.microc.2024.112068
[10] P. E. Erden, E. Kılıç, A review of enzymatic uric acid biosensors based on amperometric detection, *Talanta* **107** (2013) 312-323. https://doi.org/10.1016/j.talanta.2013.01.043
[11] R. N. Adams, Carbon paste electrodes, *Analytical Chemistry* **30** (1958) 1576. https://doi.org/10.1021/ac60141a600
[12] A. Obaid Imarah, N. Hasan, M. G. Alabbasi, ZnO-modified carbon paste electrode for electrochemical sensing of dopamine in the presence of tyrosine, *ADMET and DMPK* **13** (2025) 3010. https://doi.org/10.5599/admet.3010
[13] I. Soni, G. K. Jayaprakash, A short review on the analysis of the adsorptive behavior of surfactants at carbon paste electrodes for electrochemical sensing, *Journal of Molecular Liquids* **388** (2023) 122737. https://doi.org/10.1016/j.molliq.2023.122737
[14] S. Mir, N. Akbarzadeh Torbati, V. Amani, S. Tajik, H. Beitollahi, Y-Co metal-organic framework for sensitive electrochemical determination of doxorubicin hydrochloride, *ADMET and DMPK* **13** (2025) 3141. https://doi.org/10.5599/admet.3141
[15] L. Li, C. Meng, C. Xu, S. Kim, F. Wang, Morphology-engineered MOFs for advanced carbon capture and separation: From zero-dimensional particles to three-dimensional architectures, *Renewable and Sustainable Energy Reviews* **237** (2026) 117018. https://doi.org/10.1016/j.rser.2026.117018
[16] R. Chen, Y. Bao, R. Huang, H. Liu, Y. Luo, D. Zhang, MOF-based nanozymes: Rational design and biomedical applications, *Biomaterials* **333** (2026) 124201. https://doi.org/10.1016/j.biomaterials.2026.124201
[17] X. Wang, T. Zhou, X. Xu, Y. Bing, H. Jiang, Z. Song, W. Li, T. Zhang, Enhanced CO_2 sensing via anomalous adsorption of coordinating water molecules in partially activated Mg-MOF-74, *Chemical Engineering Journal* **538** (2026) 176519. https://doi.org/10.1016/j.cej.2026.176519
[18] S. Mandal, A. Mendhe, H.M. Rakhade, P.R. Bhendarkar, T. Deshmukh, I. Hussain, N.S. Barse, M. Roy, S.S. Karade, T. Park, H.S. Lee, Comprehensive review on MXenes, transition-metal oxides, MOFs, and COFs for supercapacitors: Progress, challenges, and future

solutions, *Materials Today Sustainability* **34** (2026) 101326. https://doi.org/10.1016/j.mtsust.2026.101326

[19] F. Lv, J. Chen, S. Wu, R. Sun, L. Zhang, Y. Luo, H. Zhang, D. Xu, A stable label-free electrochemical immunosensor based on AuNPs/Fe-MOFs/COOH-GO composites for the detection of non-small cell lung cancer marker CYFRA21-1, *Microchemical Journal* **225** (2026) 118037. https://doi.org/10.1016/j.microc.2026.118037

[20] D. Wang, J. An, X. Chang, Y. Xu, J. Zhao, L. Gao, P. Zhang, X. Li, J. Nie, H. Cui, Autogenous-reduction-engineered MOF/GO hybrids as a universal ternary nanocomposite platform for simultaneous electrochemical sensing of uric acid, dopamine and ascorbic acid, *Electrochimica Acta* **225** (2026) 148711. https://doi.org/10.1016/j.electacta.2026.148711

[21] H. Ghaedamini, R. Khanal, D.S. Kim, Peroxidase-mimicking Ce–hemin–MOFs/GO composite for enzyme-free electrochemical detection of H_2O_2, *Journal of Electroanalytical Chemistry* **1002** (2025) 119744. https://doi.org/10.1016/j.jelechem.2025.119744

http://doi.org/10.5599/jese.3447